High-Order Compact Finite Difference Methods

W. F. Spotz* G. F. Carey*

Abstract

In this work we present a general approach for developing high-order compact differencing schemes by utilizing the governing differential equation to help approximate truncation error terms. As an illustrative application we consider the stream-function vorticity form of the Navier Stokes equations, and provide driven cavity results. Some extensions to treat non-constant metric coefficients resulting from mapping from a physical to a reference domain and to 3D potential problems are considered. Supporting numerical studies showing the higher-order rates of convergence and the local superconvergence at the nodes are presented.

Key words: high order, finite difference, compact.

AMS subject classifications: 47B07, 65N06, 65N15.

1 Introduction

The standard strategy for generating higher-order difference schemes is to expand the stencil (see, for example, Leonard [8] or Castillo [4]). This has the obvious disadvantages of creating larger matrix bandwidths, complicating the numerical treatment near the boundaries and increasing communication requirements for implementation on parallel computer architectures. In light of the problems caused by non-compact finite difference schemes, it is desirable to develop a class of schemes that are both high-order and compact. Hirsh [7] conducted numerical experiments with a class of high-order compact schemes in which the first and second derivatives are treated as unknowns. This results in a mixed method and the approach is different than in the present work.

*Texas Institute for Computational and Applied Mathematics, ASE-EM Department, the University of Texas at Austin

ICOSAHOM'95: Proceedings of the Third International Conference on Spectral and High Order Methods. ©1996 Houston Journal of Mathematics, University of Houston.

It is known that compact difference approximations exist for certain operators that are higher-order than standard schemes. As an example, for the 2D Laplacian, the difference coefficients at the nine grid points corresponding to the compact patch of four cells surrounding a given node can be selected so that the second-order truncation error terms cancel [19]. More generally, by utilizing the governing differential equation it is possible to produce alternative lower-derivative expressions equivalent to the higher-order truncation error terms [12]. These alternative expressions can then be differenced compactly on the stencil, and this leads to a family of compact higher-order difference schemes [9, 10, 11, 1].

In the present work we provide a general formulation and approach for developing such higher-order compact (HOC) schemes for the prototype steady elliptic diffusion and convection-diffusion problems. We consider the extension to problems with non-constant convection coefficients and apply this strategy for the decoupled stream-function vorticity formulation of the Navier-Stokes equations. Comparison studies of the higher-order compact methods and standard methods for the driven cavity problem are made. We also examine the effects of non-constant metric coefficients associated with mapping from a nonuniform grid on a physical domain to a uniform grid on a reference domain. Finally, we present a compact higher-order scheme for the Poisson equation in three dimensions.

2 High-order compact schemes

To introduce the basic idea, let us consider the elementary, steady, 1D convection diffusion equation,

$$-\frac{d^2\phi}{dx^2} + c\frac{d\phi}{dx} = f, \tag{1}$$

where ϕ is the transport variable of interest and c and f are smooth functions of x. We define $\delta_x^n \phi_i, n = 1, 2$ to be the standard central difference operator for the n-th derivative of ϕ at point i on a uniform grid of mesh size h. Central differencing (1) yields

$$-\delta_x^2 \phi_i + c_i \delta_x \phi_i - \tau_i = f_i, \tag{2}$$

where τ_i is the local truncation error at node i,

$$\tau_i = \frac{h^2}{12}\left[2c\frac{d^3\phi}{dx^3} - \frac{d^4\phi}{dx^4}\right]_i + O(h^4). \tag{3}$$

We seek to approximate the leading term in (3) and include it in the difference formulation to yield an $O(h^4)$ method. Assuming the solution is sufficiently regular, we may accomplish this by differentiating (1) to yield

$$\left.\frac{d^3\phi}{dx^3}\right|_i = \left[c\frac{d^2\phi}{dx^2} + \frac{dc}{dx}\frac{d\phi}{dx} - \frac{df}{dx}\right]_i,$$

which can be approximated compactly as

$$\left.\frac{d^3\phi}{dx^3}\right|_i = c_i\delta_x^2\phi_i + \delta_x c_i\delta_x\phi_i - \delta_x f_i + O(h^2), \tag{4}$$

and similarly

$$\begin{aligned}\left.\frac{d^4\phi}{dx^4}\right|_i &= \left[c\frac{d^3\phi}{dx^3} + 2\frac{dc}{dx}\frac{d^2\phi}{dx^2} + \frac{d^2c}{dx^2}\frac{d\phi}{dx} - \frac{d^2f}{dx^2}\right]_i, \\ &= c_i\left.\frac{\partial^3\phi}{\partial x^3}\right|_i + 2\delta_x c_i\delta_x^2\phi_i + \delta_x^2 c_i\delta_x\phi_i - \\ &\quad \delta_x^2 f_i + O(h^2).\end{aligned} \tag{5}$$

Relations (4) and (5) can be combined with (3) to yield the new truncation error expression:

$$\begin{aligned}\tau_i &= \frac{h^2}{12}\left[(c_i^2 - 2\delta_x c_i)\delta_x^2\phi_i + (c_i\delta_x c_i - \delta_x^2 c_i)\delta_x\phi_i - \right. \\ &\quad \left. c_i\delta_x f_i + \delta_x^2 f_i\right] + O(h^4),\end{aligned}$$

which we can use to increase the accuracy of our approximation (2). The resulting high-order compact scheme is

$$-A_i\delta_x^2\phi_i + C_i\delta_x\phi_i = F_i + O(h^4), \tag{6}$$

where

$$A_i = 1 + \frac{h^2}{12}\left(c_i^2 - 2\delta_x c_i\right), \tag{7}$$

$$C_i = c_i + \frac{h^2}{12}\left(\delta_x^2 c_i - c_i\delta_x c_i\right), \tag{8}$$

$$F_i = f_i + \frac{h^2}{12}\left(\delta_x^2 f_i - c_i\delta_x f_i\right). \tag{9}$$

The asymptotic convergence of the HOC formula obtained by dropping the $O(h^4)$ term from (6) has been verified previously [17]. We present here convergence results for the model problem $c(x) = 10$, $f(x) = 0$ on $(0,1)$ with boundary conditions $\phi(0) = 0$, $\phi(1) = 1$, which has exact solution $\phi = \frac{e^{cx}-1}{e^c-1}$. Figure 1 shows the experimental

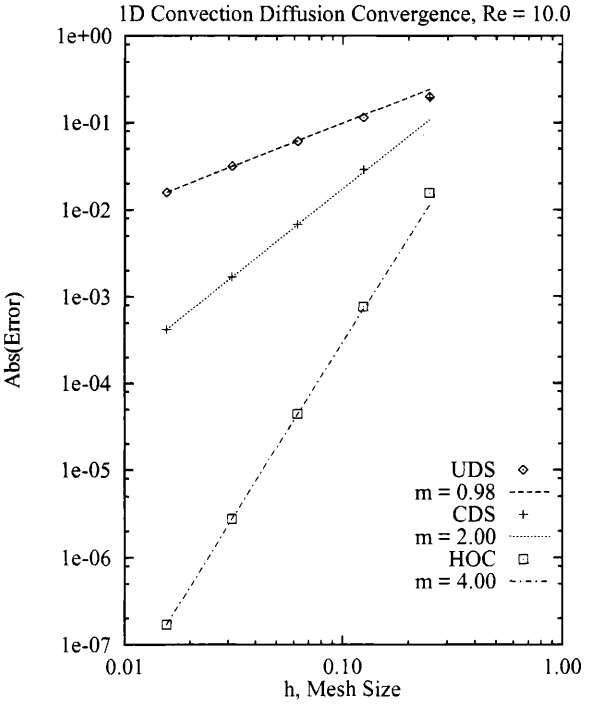

Figure 1: Convergence for 1D convection diffusion, $c = 10$.

asymptotic convergence rate m of the error E at the point $x = 0.75$ for the central difference scheme (CDS), upwind difference scheme (UDS) and the HOC scheme, computed by using the results for the meshes $h = \frac{1}{32}, h = \frac{1}{64}$. These experimental rates match the theoretical rates.

In addition to greater accuracy, HOC schemes may suppress or eliminate spurious numerical oscillations that arise in more standard lower-order schemes. For example, the HOC scheme for the homogeneous 1D convection-diffusion equation with constant convection has been proven non-oscillatory [12, 15] for all values of the product ch. This is demonstrated in Figure 2 for the case $c = 50$, $h = 1/8$, which clearly violates the well-known cell-Peclet condition, $ch < 2$. Obviously, the CDS solution exhibits non-physical oscillations in the solution, while the HOC solution is smooth.

The curves in Figure 3 correspond to bounds on the condition number for each of the 3 schemes (CDS, UDS, and HOC) for the 1D convection diffusion problem. Here, we have graphed the bound as a function of cell-Peclet number ch. For a given ch the values of the curves give condition number bounds for large N (small h) for each of the respective methods. Clearly, utilizing the HOC correction terms results in a slightly higher condition number, which implies that an iterative solver should require more itera-

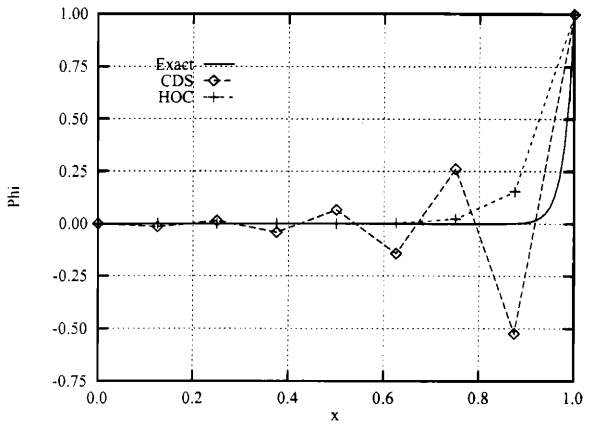

Figure 2: CDS and HOC solutions for $c = 50$, $h = 1/8$.

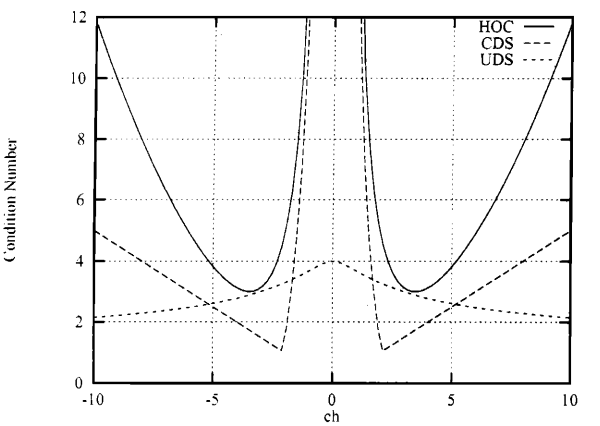

Figure 3: Condition numbers for CDS, UDS and HOC in 1D as a function of *ch*.

tions to solve an HOC system than it would for CDS or UDS systems for the same problem data and grid. Somewhat surprisingly, however, HOC formulations have been demonstrated [16] to solve *faster* than CDS or UDS using gradient-type solvers. This may indicate that HOC eigenvalues are more tightly clustered or that HOC is particularly well-suited for diagonal scaling, which was utilized in the aforementioned experiments. This result, coupled with the fact that HOC schemes allow for much coarser grids, give HOC schemes a considerable performance advantage over more conventional schemes.

3 Stream function vorticity

As an illustrative practical application we consider the HOC solution of the stream function (ψ)/vorticity (ζ) form of the 2D Navier-Stokes equations for steady, incompressible flow. The governing equations are

$$-\nabla^2\psi = \zeta, \tag{10}$$

$$-\nabla^2\zeta + Re\boldsymbol{V}\cdot\nabla\zeta = f, \tag{11}$$

where f is a forcing function, the velocity $\boldsymbol{V} = u\hat{\boldsymbol{\imath}} + v\hat{\boldsymbol{\jmath}}$, where $\hat{\boldsymbol{\imath}}$ and $\hat{\boldsymbol{\jmath}}$ are unit vectors in the x and y directions, respectively, and $Re = \frac{UL}{\nu}$ is the Reynolds number, with U a characteristic velocity, L a characteristic length scale, and ν the kinematic viscosity of the fluid. The governing equations are augmented by the auxiliary relations

$$u = \frac{\partial\psi}{\partial y}, \quad v = -\frac{\partial\psi}{\partial x}. \tag{12}$$

For the purposes of this study, we will consider wall boundary conditions, as these present some difficulty in maintaining high-order accuracy. The velocity relationships (12) can be used to relate any velocity boundary conditions to the stream function. For a wall boundary moving tangent to its surface with a constant velocity V_w, the no-slip, no-penetration condition becomes

$$\frac{\partial\psi}{\partial n} = \pm V_w, \quad \frac{\partial\psi}{\partial s} = 0, \tag{13}$$

where n is the direction normal to the wall, and s is tangent to the wall. The latter equation implies ψ is constant on the boundary. Transport equations (10) and (11), together with velocity relations (12) plus boundary conditions (13) complete the mathematical description of the fully coupled stream-function vorticity problem.

3.1 HOC formulas

The HOC approximation to this system of equations can be derived in the same manner as for 1D convection diffusion and can be found in [18]. The HOC scheme for (10) is

$$-\left[\delta_x^2 + \delta_y^2 + \frac{h^2}{6}\delta_x^2\delta_y^2\right]\psi_{ij} = \left[1 + \frac{h^2}{12}\left(\delta_x^2 + \delta_y^2\right)\right]\zeta_{ij} + O(h^4). \tag{14}$$

The HOC approximation for (11) is more complicated due to the non-constant convection velocity. It can be expressed conveniently in the form

$$-A_{ij}\delta_x^2\zeta_{ij} - B_{ij}\delta_y^2\zeta_{ij} + C_{ij}\delta_x\zeta_{ij} + D_{ij}\delta_y\zeta_{ij} - \frac{h^2}{6}\left[\delta_x^2\delta_y^2 - c_{ij}\delta_x\delta_y^2 - d_{ij}\delta_x^2\delta_y - G_{ij}\delta_x\delta_y\right]\zeta_{ij} = F_{ij} + O(h^4), \tag{15}$$

where the coefficients A_{ij}, B_{ij}, C_{ij}, D_{ij}, F_{ij} and G_{ij} are given by

$$\begin{aligned}
A_{ij} &= 1+\frac{h^2}{12}\left(c_{ij}^2-2\delta_x c_{ij}\right),\\
B_{ij} &= 1+\frac{h^2}{12}\left(d_{ij}^2-2\delta_y d_{ij}\right),\\
C_{ij} &= c_{ij}+\frac{h^2}{12}\left[\delta_x^2+\delta_y^2-c_{ij}\delta_x-d_{ij}\delta_y\right]c_{ij},\\
D_{ij} &= d_{ij}+\frac{h^2}{12}\left[\delta_x^2+\delta_y^2-c_{ij}\delta_x-d_{ij}\delta_y\right]d_{ij},\\
F_{ij} &= f_{ij}+\frac{h^2}{12}\left[\delta_x^2+\delta_y^2-c_{ij}\delta_x-d_{ij}\delta_y\right]f_{ij},\\
G_{ij} &= \delta_y c_{ij}-c_{ij}d_{ij}+\delta_x d_{ij},
\end{aligned}$$

and we let $c_{ij} = Re \cdot u_{ij}$, and $d_{ij} = Re \cdot v_{ij}$. We must also approximate the velocities u and v to a consistent degree of accuracy with respect to the rest of the numerical approximation. The HOC formulas are

$$u_{ij} = \delta_y\psi_{ij}+\frac{h^2}{6}\left(\delta_y\zeta_{ij}+\delta_x^2\delta_y\psi_{ij}\right)+O(h^4), \quad (16)$$

$$v_{ij} = -\delta_x\psi_{ij}-\frac{h^2}{6}\left(\delta_x\zeta_{ij}+\delta_x\delta_y^2\psi_{ij}\right)+O(h^4), \quad (17)$$

which are to be used in the vorticity transport equation.

Compact approximations to the normal boundary condition $\frac{\partial\psi}{\partial n} = \pm V_w$ that maintain the same high-order of accuracy present a nontrivial challenge. This relationship requires one-sided differencing of ψ which in turn yields truncation error terms of $O(h)$, $O(h^2)$, and $O(h^3)$ which must be approximated compactly to yield an $O(h^4)$ method. Still, such an approximation is possible. For example, consider a vertical wall on the left side of a rectangular cavity. After some algebraic manipulation, the HOC approximation to $-\left.\frac{\partial\psi}{\partial x}\right|_{1j} = v_{1j}$ is

$$\begin{aligned}
-\delta_x^+\psi_{1j}-\Big[&\frac{h}{2}+\frac{h^2}{6}\delta_x^+-\\
&\frac{h^3}{24}\left(Re\ v_{1j}\delta_y-\delta_y^2\right)\Big]\zeta_{1j}+O(h^4)=\\
&v_{1j}-\frac{h^3}{24}\left(\delta_x^+\delta_y^2 v_{1j}-f_{1j}\right)+O(h^4),
\end{aligned} \quad (18)$$

where the operator δ_x^+ denotes one-sided forward differencing. Similar conditions can be derived for the remaining three walls of a rectangular cavity and lower-order expressions (which will be needed later) may be obtained by dropping the appropriate higher-order terms in (18).

Boundary conditions at the corners are handled in a similar manner. The restricted geometry at the corners prevents the derivation of a fourth-order compact formula, but a third-order approximation is possible. For example, at the upper left corner (x_1, y_M), we can approximate $\frac{\partial\psi}{\partial n}$ in both the horizontal and vertical directions. Summing these results and replacing high-order terms with appropriate difference expressions, we obtain

$$\begin{aligned}
\left[\delta_x^+ + \delta_y^-\right]\psi_{1M}+\frac{h}{2}\zeta_{1M}+\frac{h^2}{6}\left[\delta_x^+-\delta_y^-\right]\zeta_{1M} =\\
-u_{1M}-v_{1M}-\\
\frac{h^2}{6}\left[\delta_x^+\delta_y^- u_{1M}+\delta_x^+\delta_y^- v_{1M}\right]+O(h^3).
\end{aligned} \quad (19)$$

3.2 HOC results

In the present work we use a decoupled block iterative scheme to solve the stream function vorticity system. Solution proceeds from an initial vorticity iterate by first solving (14) for ψ with Dirichlet boundary conditions, using the current values for ψ and ζ to update the velocities using (16) and (17). Then these values are used in (15), (18), and (19) to solve for ζ, at which point the iterative procedure can be repeated. In practice, successive iterates may have to be under-relaxed in order to converge. That is to say, if ψ' is the stream function computed from the first half of the decoupled algorithm, then ψ at iteration level $n+1$ is given by

$$\psi^{n+1} = \omega\psi' + (1-\omega)\psi^n,$$

where ω is the relaxation factor.

To illustrate the $O(h^4)$ accuracy, we construct a test problem with known solution by specifying the stream-function

$$\psi = -8(x-x^2)^2(y-y^2)^2$$

on the unit square $\Omega = (0,1)^2$. The corresponding vorticity function, derived from equation (10), is

$$\zeta = 16[(6x^2-6x+1)(y-y^2)^2+(x-x^2)^2(6y^2-6y+1)],$$

and the velocities, derived from (12) are

$$\begin{aligned}
u &= -16(x-x^2)^2(y-y^2)(1-2y),\\
v &= 16(x-x^2)(1-2x)(y-y^2)^2.
\end{aligned}$$

This model problem was designed so that the no-slip, no-penetration condition holds for the velocities u and v on the boundary. The flow is driven by the forcing function f, which is constructed by substituting the above functions ζ, u and v in (11). In the following numerical test we solve the linear Stokes flow problem, $Re = 0$, to better isolate the effect of the choice of boundary condition accuracy. The fourth-order scheme is applied in the interior and $O(h^2)$, $O(h^3)$ and $O(h^4)$ boundary conditions are

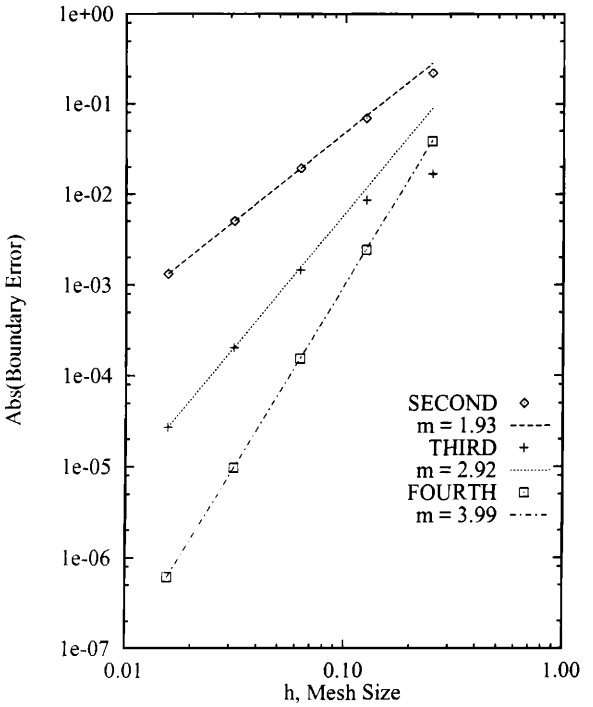

Figure 4: HOC vorticity error convergence plot on the boundary for the (ψ, ζ) model problem with $Re = 0$.

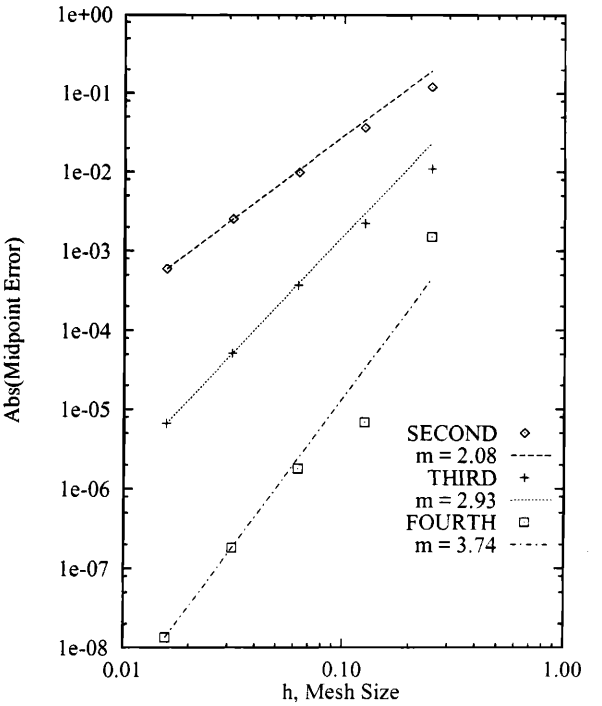

Figure 5: HOC vorticity error convergence plots at the midpoint for the (ψ, ζ) model problem with $Re = 0$.

compared. Figures 4 and 5 show the vorticity error at a representative boundary point ($x = 0.5$, $y = 0$), and at the midpoint ($x = y = 0.5$) respectively for a succession of meshes and for each of the following implementations of the wall boundary conditions: $O(h^2)$ boundary conditions are labeled "SECOND" in the plots, $O(h^3)$ boundary conditions are labeled "THIRD," and $O(h^4)$ boundary conditions are labeled "FOURTH." The experimental convergence rates at the stated points are computed as in the 1D example, and are seen to agree with the theoretical rates.

The second problem studied was the lid-driven cavity flow, a standard test case for steady Navier-Stokes computations with numerous published results that can be used for comparison purposes. This problem is complicated, however, by the presence of two corner singularities [6]. We consider the unit cavity again with horizontal lid velocity $u = 1, v = 0$ along the top. On the remaining sides $u = v = 0$.

The HOC (ψ, ζ) approximation provides highly accurate results for the driven cavity when $O(h^3)$ boundary conditions are used. Somewhat surprisingly, though, $O(h^4)$ boundary conditions result in isolated oscillations in the vorticity on the moving wall. More complete results can be found in [18], but some conclusions are summarized here. The fourth-order boundary conditions can lead to oscillations in the vorticity solution along (and only along) the moving wall if the cell-Peclet condition, $Re \cdot h < 2$ is violated. An example of this is depicted in Figure 6. This is most likely due to the presence of the convective term tangent to the wall in (18). Supporting this conclusion is the fact that no oscillations appear on stationary walls (where this term is zero) and no oscillations appear at all if third-order BCs are utilized by neglecting the high-order term which contains the convective contribution.

For this reason, third-order boundary conditions were used to solve the driven cavity problem. In a similar vein, at the two upper corners where singularities exist, lower-order corner boundary conditions worked best. Therefore, $O(h^2)$ BCs, the lowest-order approximation which still utilize the vorticity were used at the corners.

As an example of HOC driven cavity results, we present results for the relatively convective case of $Re = 1000$ on a coarse grid of 41×41. For such data, the CDS solution is wildly oscillatory and not included. The UDS yields smooth but inaccurate results. We compare our HOC results to the fine-grid (129×129) second-order results of Ghia, *et al* [5]. Figures 7 and 8 show cross-sections of the

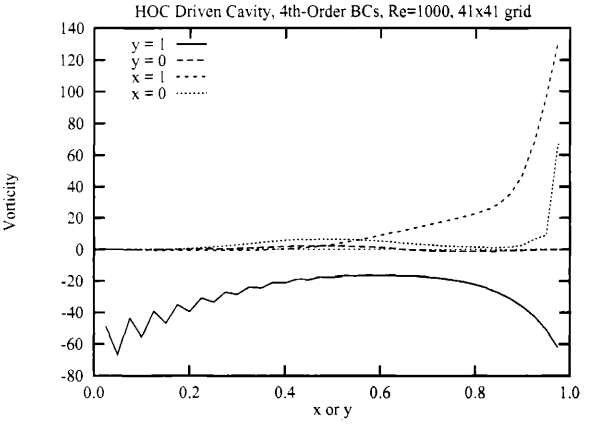

Figure 6: Vorticity on the four boundaries of the driven cavity problem for $Re = 1000$ and $O(h^4)$ boundary conditions.

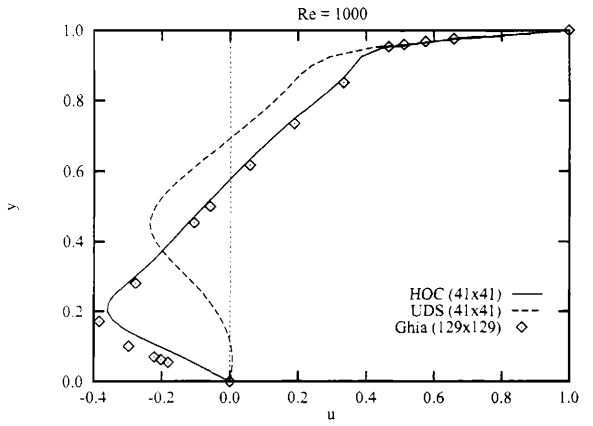

Figure 7: Driven cavity results for the horizontal velocity component along the vertical centerline, $Re = 1000$.

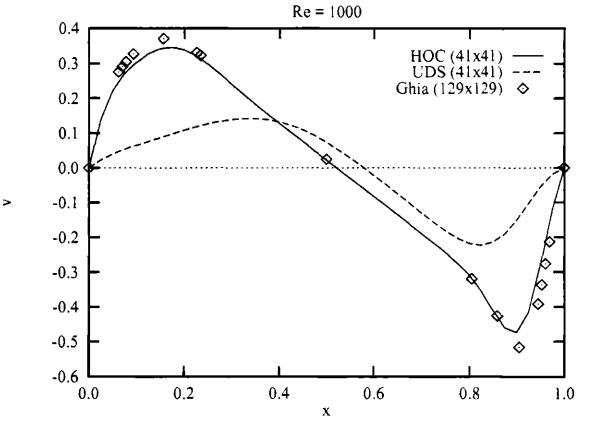

Figure 8: Driven cavity results for the vertical velocity component along the horizontal centerline, $Re = 1000$.

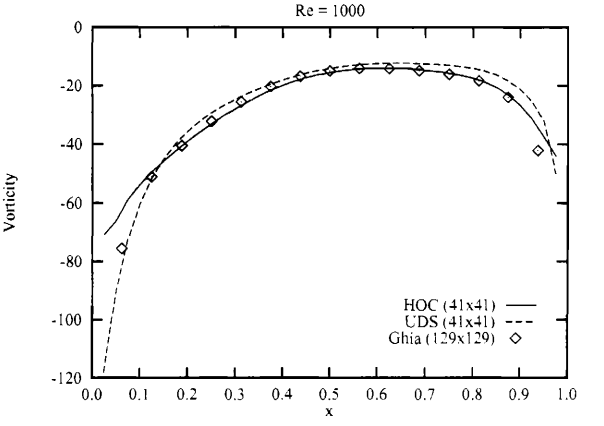

Figure 9: Driven cavity results for the vorticity along the moving wall, $Re = 1000$ and $O(h^3)$ side boundary conditions.

velocities on the interior of the cavity, and Figure 9 shows the vorticity along the moving wall. Clearly, the HOC results are far superior to the UDS results and achieve accuracy comparable to the reference results using roughly 10% of the number of grid points.

4 Some extensions

The HOC examples shown so far give promising results, but there are some undesirable restrictions. For example, the approximations described above require uniformly spaced meshes. Also, HOC schemes offer the greatest promise for 3D applications, but the algebraic complexity of these numerical schemes grow with problem dimension and complexity. In this section we hope to address some of these issues and give an indication of future areas of research in the area of HOC finite differences.

4.1 Nonuniform grids in 1D

It is common practice in numerical methods to map the given problem from the physical domain Ω to a reference domain $\hat{\Omega}$ and to solve the transformed problem approximately on $\hat{\Omega}$ using a uniform difference grid. Since the HOC methods have been constructed for uniform grids, this mapping formulation is a natural approach for extending the ideas to nonuniform grids. However, as we shall demonstrate, there are additional considerations that must be addressed for the compact schemes to remain high-order.

As a first step, we restrict the treatment to the 1D case and again consider the model convection diffusion equation

$$-\frac{d^2\phi}{dx^2} + u(x)\frac{d\phi}{dx} = g(x), \tag{20}$$

with the familiar boundary conditions $\phi(0) = 0$, $\phi(1) = 1$. Let us construct a map $x = x(\xi)$ to transform (20) from a graded mesh on $0 \le x \le 1$ to a uniform mesh on $0 \le \xi \le 1$. The transformed equation is simply

$$-\left(\frac{d\xi}{dx}\right)^2 \frac{d^2\hat{\phi}}{d\xi^2} + \left(\hat{u}\frac{d\xi}{dx} - \frac{d^2\xi}{dx^2}\right)\frac{d\hat{\phi}}{d\xi} = \hat{g}, \tag{21}$$

where $\hat{\phi}(\xi) = \phi(x(\xi))$, $\hat{u}(\xi) = u(x(\xi))$, $\hat{g}(\xi) = g(x(\xi))$, and the metric coefficients $\frac{d\xi}{dx}$ and $\frac{d^2\xi}{dx^2}$ now enter the formulation. It is well known that the metric coefficients in (21) must be approximated accurately. Here, we are specifically interested in retaining accuracy within the high-order compact framework.

Provided the map is regular and non-degenerate (so that $\frac{d\xi}{dx} \neq 0$) we can write (21) conveniently in the form

$$-\frac{d^2\hat{\phi}}{d\xi^2} + c(\xi)\frac{d\hat{\phi}}{d\xi} = f(\xi), \tag{22}$$

where

$$c(\xi) = \frac{\hat{u}\frac{d\xi}{dx} - \frac{d^2\xi}{dx^2}}{\left(\frac{d\xi}{dx}\right)^2}, \quad f(\xi) = \frac{\hat{g}}{\left(\frac{d\xi}{dx}\right)^2}. \tag{23}$$

Equation (22) is in exactly the same form as (1), so we can apply the previous HOC scheme in (6) to the mapped problem. However, note that the coefficients in (7)–(9) involve differences of the rational expressions in (23) and these, in turn, contain first and second derivatives of the transformation function. This implies not only more computational work to implement (6), but also raises some important open questions concerning the effect of the transformation and difference approximations in the compact formulation.

Consider the model 1D test problem again. To illustrate the idea let us introduce the mapping function

$$x(\xi) = \xi + \frac{\gamma}{\pi}\sin\pi\xi, \quad 0 \le \xi \le 1, \tag{24}$$

where γ is the grading parameter. The map is invertible for $|\gamma| < 1$; $\gamma > 0$ corresponds to compression (clustering) to the right and similarly to the left for $\gamma < 0$. In the following calculations we choose $\gamma = \frac{1}{2}$ which corresponds to a moderate grading to the right.

The test problem was computed on a sequence of uniformly refined grids $h = \frac{1}{4}, \frac{1}{8}, \ldots \frac{1}{64}$ for $u = 20$. The error

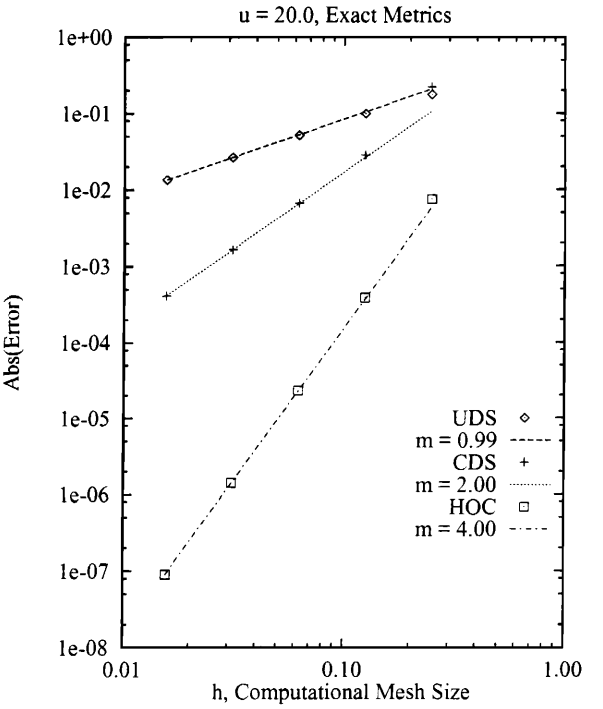

Figure 10: Convergence results for 1D convection diffusion on a nonuniform grid with exact metrics, $u = 20$.

was computed in the same manner as the 1D example on uniform grids at representative grid point $x_i = x(\xi_i = 0.75)$, and is graphed in Figure 10 against mesh size h on a log-log scale for the central difference scheme (CDS), upwind difference scheme (UDS) and high-order compact (HOC) scheme. The calculations for the high-order scheme utilize full knowledge of the analytic map (24) to compute the metric derivatives $\frac{d\xi}{dx}$ and $\frac{d^2\xi}{dx^2}$ exactly, and the optimal superconvergent $O(h^4)$ rate is obtained.

In practice, the map may not be specified analytically and the metric coefficients may have to be differenced. We examine the effect of this approximation using the grid from the preceding test. That is, we take precisely the nonuniform grid generated by (24) and evaluate the entries in (23) at each point by locally differencing for $\frac{d\xi}{dx}$ and $\frac{d^2\xi}{dx^2}$. This would be a natural approach given an arbitrary graded mesh $\{x_i\}$. The results for the compact formula (6) with this approximation are summarized in Figure 11. Note that the effect of approximating the metric derivatives by differences is to degrade the asymptotic rate of the HOC scheme reducing it to $O(h^2)$, although for the case $u = 20$ the HOC scheme is almost an order of magnitude more accurate than for the CDS.

This is encouraging, but the mesh gradation is mild and

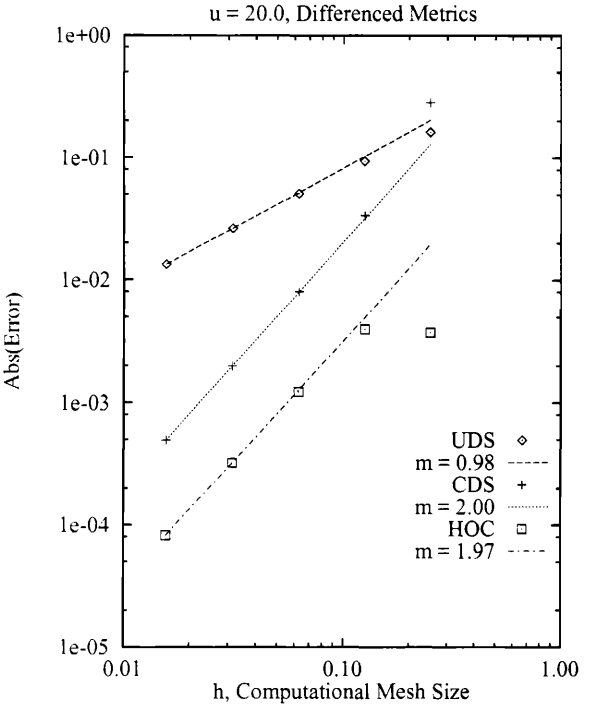

Figure 11: Convergence results for 1D convection diffusion on a nonuniform grid with differenced metrics, $u = 20$.

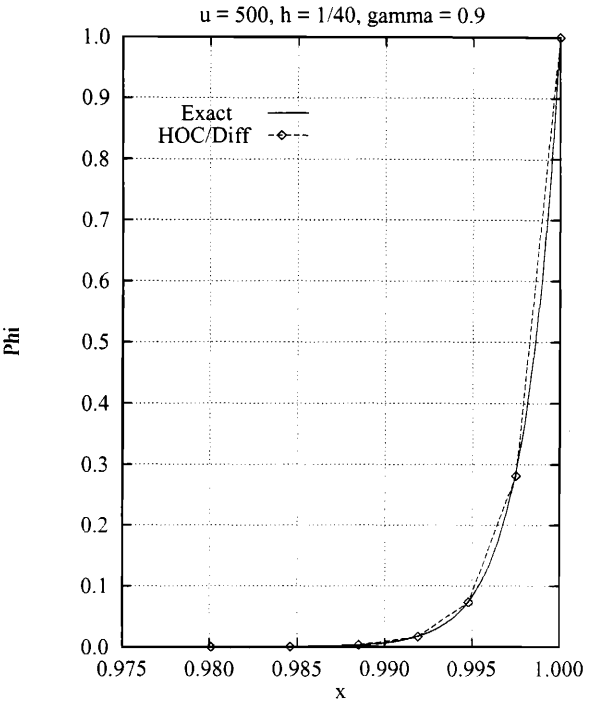

Figure 12: Boundary layer results for the HOC scheme with differenced metrics, $u = 500$, $\gamma = 0.9$, and $h =$.

the Peclet number of 50 is quite moderate so the boundary layer near $x = 1$ is relatively modest. The ability of the method to function with more strongly graded meshes and at higher convection levels is therefore relevant. In fact, if faithful representation of the layer structure is desired then the mesh should be graded so that there are a few grid points guaranteed to lie within the layer. Figure 12 shows the boundary layer results for 1D convection diffusion on a nonuniform grid with $u = 500$, $\gamma = 0.9$ and $h = 1/40$. Clearly there is excellent agreement with the exact solution using only a few points to resolve the layer.

If the map $x(\xi)$ is not known explicitly, it may have been generated by the numerical solution of some differential equation (as in PDE grid generators). It is then possible to recover the full $O(h^4)$ estimate suggested by (6) in a manner analogous to the way in which the HOC scheme was developed for the governing transport equation. To illustrate this idea, let us introduce the boundary value problem

$$\frac{d^2x}{d\xi^2} + \pi^2 x = \pi^2 \xi, \tag{25}$$

with boundary conditions $x(0) = 0, x(1) = 1$, which corresponds to a Helmholtz PDE grid generator in 1D with a positive source term proportional to ξ. The exact solution is precisely the grading function $x(\xi)$ in (24). Let us assume now that the grid (and indirectly the map) is generated by solving (25) accurately using a uniform grid. Now (25) can be used as an auxiliary relation for the difference approximation of the metrics $\frac{d\xi}{dx}$ and $\frac{d^2\xi}{dx^2}$ at grid point i. Specifically, we can use HOC methodology to derive

$$\left.\frac{d\xi}{dx}\right|_i = \frac{1}{\left(1 + \frac{h^2\pi^2}{6}\right)\delta_\xi x_i - \frac{h^2\pi^2}{6}},$$

$$\left.\frac{d^2\xi}{dx^2}\right|_i = \frac{-\pi^2(\xi_i - x_i)}{\left[\left(1 + \frac{h^2\pi^2}{6}\right)\delta_\xi x_i - \frac{h^2\pi^2}{6}\right]^3},$$

which are $O(h^4)$ approximations to the metric derivatives of interest [17].

Figure 13 shows the convergence results for the case where the metrics are computed using this auxiliary equation[1]. The HOC method does in fact recover the optimal $O(h^4)$ result.

[1] As an alternative to utilizing a relation such as (25) in this way, one could simply use more adjacent grid points to approximate the metric derivatives more accurately. While this is counter to the goals of a compact representation, it may be acceptable since the grid metric coefficients can be computed explicitly prior to constructing the HOC stencils. This implies that the HOC scheme (6) can be constructed even for very irregular grids in 1D where there is no

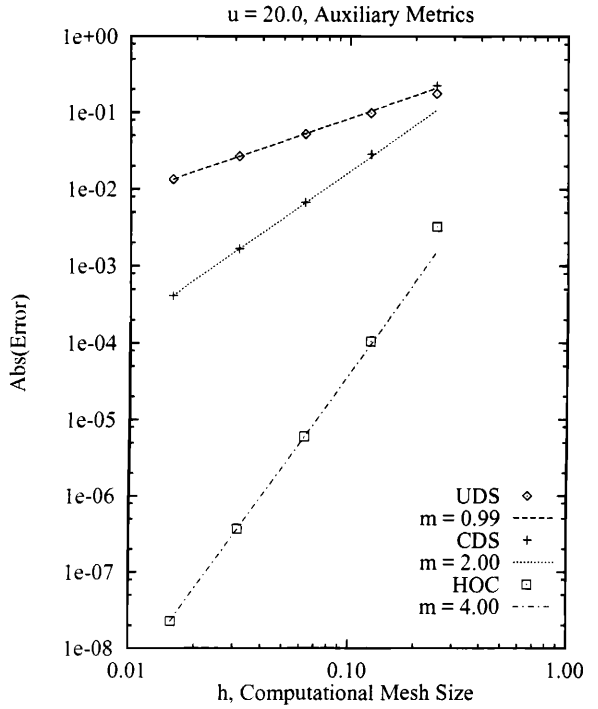

Figure 13: Convergence results for 1D convection diffusion on a nonuniform grid with approximated metrics using an auxiliary equation, $u = 20$.

4.2 3D Poisson

An $O(h^6)$ compact scheme for Laplace's equation in 2D has been available in the literature for some time [19, 2]. Here, we present a construction for the 3D Poisson equation on a structured grid, leading to an $O(h^6)$ scheme for the case where the necessary derivatives of the source term can be obtained explicitly and $O(h^4)$ where differencing is used to compute these derivatives.

Consider the Poisson equation

$$\nabla^2 \phi = f, \tag{26}$$

for specified forcing function f in 3D domain Ω with appropriate boundary conditions on $\partial\Omega$. Using the same approach as in the rest of this work, a sixth-order HOC approximation to (26) on a uniform grid is

$$\left[\delta_x^2 + \delta_y^2 + \delta_z^2 + \frac{h^2}{6}\left(\delta_x^2\delta_y^2 + \delta_y^2\delta_z^2 + \delta_x^2\delta_z^2\right) + \frac{h^4}{30}\delta_x^2\delta_y^2\delta_z^2\right]\phi_{ijk} = f_{ijk} + \frac{h^2}{12}\nabla^2 f_{ijk} + \frac{h^4}{360}\nabla^4 f_{ijk} + \frac{h^4}{180}\left(\frac{\partial^4 f}{\partial x^2 \partial y^2} + \frac{\partial^4 f}{\partial y^2 \partial z^2} + \frac{\partial^4 f}{\partial x^2 \partial z^2}\right)_{ijk} \tag{27}$$

where ∇^4 is the bi-harmonic operator. The resulting stencil involves all 27 grid points surrounding an arbitrary interior node, including the 8 corner points, and is depicted in Figure 14, along with the resulting matrix coefficient entries.

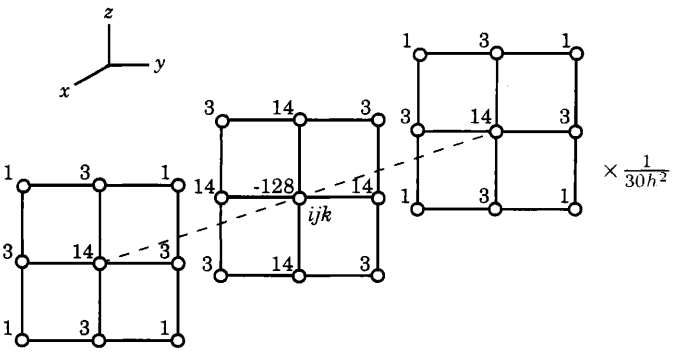

Figure 14: 27-Point $O(h^6)$ HOC Stencil.

Equation (27) is $O(h^6)$ accurate only if the higher-order derivatives of f can be computed analytically. If this is not the case (equation (10) is a good example) then we are limited to $O(h^4)$. Neglecting the $O(h^4)$ terms from (27) yields a simpler stencil, depicted in Figure 15, that does not involve the 8 corner nodes of the associated cube.

As a 3D test case we constructed a problem with a non-zero forcing function. For the domain $\Omega = (0,1)^3$ with $\phi = 0$ on the entire boundary $\partial\Omega$ and forcing function

$$f = -3\pi^2 \sin \pi x \sin \pi y \sin \pi z,$$

the exact solution to (26) is

$$\phi = \sin \pi x \sin \pi y \sin \pi z.$$

The results for central differencing, fourth-order compact (HOC4) and sixth-order compact (HOC6) are presented in Figure 16. The sequence of mesh sizes is $h = \frac{1}{2}, \frac{1}{4}, \frac{1}{6}, \frac{1}{8},$

specified algebraic mapping function or PDE grid generator *a priori*. For example, the mapping $x(\xi)$ could be constructed for a set of points $\{x_i\}$ using the Lagrange basis on the domain.

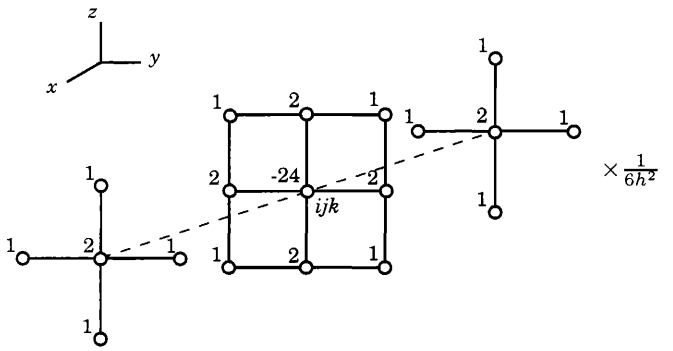

Figure 15: 19-Point $O(h^4)$ HOC Stencil.

and $\frac{1}{10}$ and rather than measure the error at a single point, we examine a more global measure of the error, namely

$$E = \left(\frac{\sum_{ijk} e_{ijk}^2}{N} \right)^{1/2},$$

where N is the total number of grid points and $e_{ijk} = o_{ijk} - o(x_i, y_j, z_k)$. The predicted convergence rates were achieved.

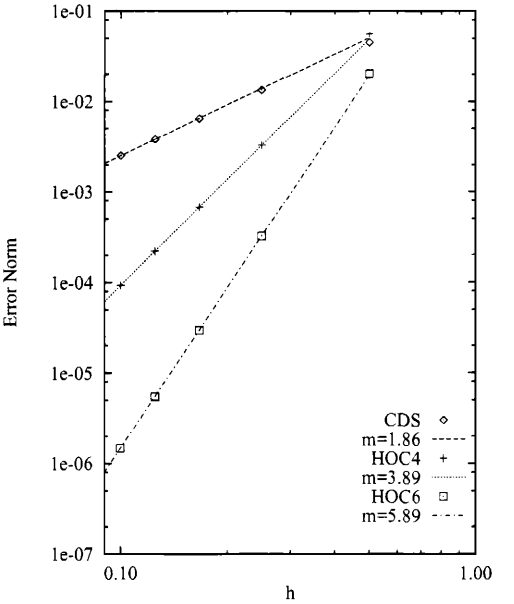

Figure 16: Convergence Rates for 3D model problem.

5 Conclusions

In this study we describe a strategy for developing HOC difference formulas and demonstrate the performance of such schemes for representative problems in one, two, and three dimensions. The methods are appealing since they provide high accuracy on coarse grids and this can significantly impact CPU time, particularly in 2D and 3D applications such as the viscous flow example where results on a 41×41 HOC grid are superior to those in the literature for a 129×129 grid using a more conventional method. We have also shown that the methods may be more robust insofar as numerical oscillations are concerned.

Some extensions to nonuniform grids obtained by mapping are also considered and we are presently extending the approach to certain classes of nonlinear problems. The present treatment considers only equilibrium problems but clearly can be applied to evolution PDEs. Indeed there are often related studies in the literature (e.g., see [8, 14]). In some sense the ideas here are related to superconvergence theory which is a topical research area in finite element analysis, but primarily as a post-processing technique [3]. There have also been some related investigations of Petrov-Galerkin finite element schemes where similar high nodal accuracy is attained [13, 20]. Clearly, there are many issues that still need to be investigated with regard to these higher-order compact schemes. These include their use for multi-grid problems, post-processing strategies and mixed methods (for example, we have recently extended the method to mixed methods for elliptic problems). Finally, we remark that the main difficulty we perceive is the formidable algebra that must be carried out to formulate the method for more complex PDEs. Symbolic manipulators hold some promise here but have not produced useful results to date.

Acknowledgments

This research has been supported in part by the industrial associates of the EOGRR at the University of Texas and by the Texas Advanced Technology Programs.

References

[1] S. Abarbanel and A. Kumar. Compact higher-order schemes for the Euler equations. *Journal of Scientific Computing*, 3:275–288, 1988.

[2] L.M. Adams, R.J. Leveque, and D.M. Young. Analysis of the SOR iteration for the 9-point Laplacian.

SIAM Journal on Numerical Analysis, 25(5):1156–1180, October 1988.

[3] G.F. Carey and R.J. MacKinnon. Superconvergence and finite element post processing. In R. Lewis, editor, *NUMETA*, Swansea, U.K., July 6–10 1987. Pineridge Press.

[4] J.E. Castillo, J.M. Hyman, M.J. Shashkov, and S. Steinberg. The sensitivity and accuracy of fourth order finite difference schemes on nonuniform grids in one dimension. *Journal of Computers & Mathematics with Applications*, to appear.

[5] U. Ghia, K.N. Ghia, and C.T. Shin. High *Re* solutions for incompressible flow using Navier-Stokes equations and a multi-grid method. *Journal of Computational Physics*, pages 387–411, 1982.

[6] P. Grisvard, editor. *Singularities and Constructive Methods for Their Treatment: Proceedings of the Conference held in Oberwolfach, West Germany.* Springer-Verlag, New York, 1985.

[7] R.S. Hirsh. Higher order accurate difference solution of fluid mechanics problems by a compact differencing technique. *Journal of Computational Physics*, 9(1):90–109, 1975.

[8] B.P. Leonard. A stable and accurate convective modeling procedure based on quadratic upstream interpolation. *Computer Methods in Applied Mechanics and Engineering*, 19:59–98, 1979.

[9] R.J. MacKinnon and G.F. Carey. Analysis of material interface discontinuities and superconvergent fluxes in finite difference theory. *Journal of Computational Physics*, 75(1):151–167, 1988.

[10] R.J. MacKinnon and G.F. Carey. Superconvergent derivatives: A Taylor series analysis. *International Journal for Numerical Methods in Engineering*, 28:489–509, 1989.

[11] R.J. MacKinnon and G.F. Carey. Nodal superconvergence and solution enhancement for a class of finite element and finite difference methods. *SIAM Journal on Scientific and Statistical Computing*, 11(2):343–353, March 1990.

[12] R.J. MacKinnon and R.W. Johnson. Differential equation based representation of truncation errors for accurate numerical simulation. *International Journal for Numerical Methods in Fluids*, 13:739–757, 1991.

[13] R.J. MacKinnon and M.A. Langerman. A compact high-order finite-element method for elliptic transport problems with variable coefficients. *Numerical Methods for Partial Differential Equations*, 10:1–19, 1994.

[14] B.J. Noye. Compact unconditioanlly stable finite difference method for transient one-dimensional advection-diffusion. *Communications in Applied Numerical Methods*, 7(7):501–512, October 1991.

[15] W.F. Spotz. Superconvergent finite difference methods with applications to viscous flow. Master's thesis, University of Texas at Austin, 1991.

[16] W.F. Spotz. *High-Order Compact Finite Difference Schemes for Computational Mechanics.* PhD thesis, University of Texas at Austin, December 1995.

[17] W.F. Spotz and G.F. Carey. High-order compact schemes for nonuniform grids. *IMA Journal of Numerical Analysis*, Submitted May, 1994.

[18] W.F. Spotz and G.F. Carey. High-order compact scheme for the stream-function vorticity equations. *International Journal for Numerical Methods in Engineering*, to appear.

[19] A.I. van de Vooren and A.C. Vliegenthart. On the 9-point difference formula for Laplace's equation. *Journal of Engineering Mathematics*, 1:187–202, 1967.

[20] J.J. Westerink and D. Shea. Consistent higher degree Petrov-Galerkin methods for the solution of the transient convection-diffusion equation. *International Journal for Numerical Methods in Engineering*, 28:1077–1101, 1989.